Contribution of close collisions to the Barkas effect: The classical picture

N. R. Arista,[1] P. L. Grande,[2] and A. F. Lifschitz[3]
[1]*División Colisiones Atómicas, Centro Atómico Bariloche and Instituto Balseiro, Comisión Nacional de Energía Atómica, 8400 S. C. de Bariloche, Argentina*
[2]*Instituto de Física da Universidade Federal do Rio Grande do Sul, Avenida Bento Goncalves 9500, 91501-970, Porto Alegre, RS, Brazil*
[3]*Laboratoire de Physique des Gaz et des Plasmas, Université Paris Sud, F-91405 Orsay Cedex, France*
(Received 17 May 2004; published 22 October 2004)

According to a previous estimation made by Lindhard [Nucl. Instrum. Method Phys. Res. **132**, 1 (1976)] on the basis of qualitative arguments and dimensional analysis, the contribution of close collisions to the Barkas effect in the energy loss of swift ions in solids yields a significant fraction of the total effect, being almost equal to the contribution coming from distant collisions. Here the classical estimation by Lindhard is reconsidered and subjected to a tight numerical test. We analyze in quantitative terms the classical description of the Barkas effect following the line of arguments proposed by Lindhard. We consider a swift ion of charge Z_1 interacting with the electrons via a screened potential assuming spherical and nonspherical screening models. We calculate by numerical integration the differential and total transport cross sections and find an important asymmetry of both with respect to the sign of Z_1, as well as a departure from the Z_1^2 behavior. These effects are particularly important for impact parameters in the range of the classical collision radius ($r_{cl}=Z_1e^2/mv^2$). This approach clearly shows the contribution of close collisions to the Barkas effect. We analyze the behavior of the Barkas asymmetry with respect to ion charge and velocity, obtaining a good quantitative agreement with Lindhard's prediction. However, an additional term predicted for nonspherical potentials cannot be reproduced.

DOI: 10.1103/PhysRevA.70.042902 PACS number(s): 34.50.Bw, 34.50.Fa

I. INTRODUCTION

The discovery of different penetration ranges for positive and negative pions in matter made by Barkas and co-workers [1] was the first evidence of deviations of the stopping power of energetic particles from the quadratic dependence on projectile charge Z_1 predicted by the Bethe theory [2]. The origin of this difference, as proposed by Barkas, is due to higher-order terms in the perturbative Born series. The first theoretical study of this effect, made by Ashley, Ritchie, and Brandt (ARB) [3,4], was followed by other pioneering studies [5,6]. The ARB model [3] was based on the classical harmonic-oscillator model. The treatment was similar to the Bohr model [7] but the analysis was extended to second-order (Z_1^3) terms, corresponding to the polarization of the atomic oscillators, in the approximation of distant collisions. They showed that the Barkas effect is characterized by the classical parameter $gZ_1\omega_0/v^3$, where Z_1 is the bare-ion charge, ω_0 the oscillator frequency, v the particle velocity, and g a numerical constant. The contribution from close collisions was neglected in this approach.

The role of close collisions in the Barkas effect was stressed later on by Lindhard [8], who made a brief estimation using qualitative arguments also based on a classical picture of the scattering process. Using simple dimensional analysis he predicted in a general way that the effect of close collisions should scale also with the same parameter $gZ_1\omega_0/v^3$. Hence, the contribution of close collisions would almost duplicate the magnitude of the total Barkas effect.

In further studies, the effect of close collisions was calculated quantum mechanically using second-order scattering theory [9], nonlinear response theory [10], and many-body theory [11].

The question of the magnitude of the relative contributions to the Barkas effect arising from close and distant collisions has been a point of much interest and has stimulated a significant number of experimental and theoretical studies [12–18].

In this paper we will analyze in a more quantitative way the original calculation of the Barkas effect sketched by Lindhard [8], which was formulated in purely classical terms and restricted to close collisions. Since a classical treatment is used, the validity of the approach is limited by the condition $2Z_1e^2/\hbar v>1$ (i.e., the classical Bohr regime). This includes part of the range of interest for swift heavy ions. In the present analysis (as well as in the original Lindhard work) only the case of bare ions will be considered. The basic parameter in Lindhard's formulation is the quantity $\zeta=Z_1e^2\omega/mv^3$, where Z_1e is the ion charge, v its velocity, and ω a characteristic frequency of the electrons in the medium. In our description this frequency will be set equal to the plasma frequency ω_P, as we will be dealing with a free electron gas. Following Lindhard, the parameter ζ may be explained as the ratio of the two relevant quantities in the classical description: the collision radius $b_{cl}=Z_1e^2/mv^2$, and the adiabatic (or screening) length $\lambda\approx v/\omega$. As stressed by Lindhard, ζ is the only dimensionless parameter that can be constructed in a classical treatment of the scattering process for high-energy particles (in particular, this is also the parameter that appears in the logarithmic term in Bohr's energy loss formula [7]).

The purpose of this paper is to perform a detailed study of Lindhard's argument to explain the origin of the Barkas effect in close collisions and to evaluate the magnitude of its contribution.

The paper is organized as follows. In Sec. II we formulate the calculation method, present and discuss the results, and analyze the contribution of close collisions to the Barkas effect. The calculations of the transport cross section by two different methods are presented in Sec. III, and in Sec. IV we summarize the conclusions of the paper. We also include two Appendixes; the first one contains details of the induced potential and spherical average used in some of the calculations, while in the second one we further illustrate the Barkas effect using a simple but exactly solvable model.

II. CLASSICAL SCATTERING FORMULATION

A. General considerations

In the following we will consider the scattering of electrons by the screened ion potential in the center of mass system (which for practical purposes may be assumed to be fixed at the ion position). In correspondence with Lindhard's assumptions [8] we will consider the target electrons to be initially at rest, so that the relative electron-ion velocity will be equal to the ion velocity v (note that this assumption may be released using a more general transformation which considers a distribution of electron velocities in the target).

First we will calculate the differential cross section using a fully classical description, and then we will integrate the transport cross section (TCS) $\sigma_{tr}(v)$. In the case of swift ions (or as long as the electrons-at-rest assumption holds) the TCS is simply connected with the average energy loss dE/dx by $dE/dx = nmv^2\sigma_{tr}(v)$, where n is the electron density of the medium. This description may be generalized to the case of moving electrons by performing an integration over the relative electron-ion velocities in the form indicated in Ref. [19].

Following the spirit of the original Lindhard estimation, we will first use a simplified description of the scattering potential, represented as a Yukawa potential with a velocity-dependent screening parameter α, and after that a full nonspherical potential. Both functions include the bare-ion potential and the induced potential according to dielectric theory, as discussed in Appendix A.

In the case of a spherical potential, the scattering angle may be calculated as a function of the impact parameter b using the well-known expression

$$\theta(b) = \pi - 2b\int_{r_0}^{\infty} \frac{dr}{r^2\sqrt{1 - b^2/r^2 - V(r)/E}}, \tag{1}$$

where the turning point value r_0 is the root of the function $R(r) = 1 - b^2/r^2 - V(r)/E$.

The first form of the scattering potential used in these calculations was a spherically symmetric one given in the form $V(r) = -(Z_1e^2/r)\phi(x)$, where Z_1 is the ion charge and $\phi(x)$ is a screening function which scales with $x = \alpha r$. In the present calculations we used $\phi(x) = \exp(-\alpha r)$, where the screening constant was taken as $\alpha = (\pi/2)\omega_P/v$ (see Appendix A for details).

Before describing the results obtained with this approach it becomes useful to derive an interesting scaling property of the transport cross section. First, we introduce the variable $x = \alpha r$ and the parameter $b^* = \alpha b$, so that Eq. (1) becomes

$$\theta = \theta(b^*, B) = \pi - 2b^*\int_{x_0}^{\infty} \frac{dx}{x^2\sqrt{R(x)}}, \tag{2}$$

where $R(x) = 1 - b^{*2}/x^2 + 2B\phi(x)/x$, and $x_0 = \alpha r_0$ is the root of $R(x)$. In doing this transformation one finds that the two parameters that characterize the scattering process are $b^* = \alpha b$ (reduced impact parameter) and

$$B = Z_1e^2\alpha/mv^2 \tag{3}$$

(Barkas parameter). It is interesting to note that this parameter corresponds to the inverse of the reduced energy ϵ from the nuclear stopping theory.

Next, we consider the transport cross section and also scale it using $b^* = \alpha b$,

$$\sigma_{tr} = \int [1 - \cos(\theta)]2\pi b db = \frac{1}{\alpha^2}\sigma^*(B), \tag{4}$$

where $\sigma^*(B) = \int [1 - \cos(\theta)]2\pi b^* db^*$.

Finally, we consider the values of the TCS for particles ($B > 0$) and antiparticles ($B < 0$), and introduce the *Barkas factor* by

$$R_{Barkas} = \frac{\Delta\sigma_{tr}}{2\langle\sigma_{tr}\rangle} \tag{5}$$

where $\Delta\sigma_{tr}$ is the TCS difference, $\Delta\sigma_{tr} = \sigma_{tr}(|B|) - \sigma_{tr}(-|B|)$, and $\langle\sigma_{tr}\rangle = \frac{1}{2}[\sigma_{tr}(|B|) + \sigma_{tr}(-|B|)]$.

From Eq. (4) we find that R_{Barkas} is a function of the single parameter B. This is in accord with the general scaling argument given originally by Lindhard [8].

B. Calculations

Using the described approach we have performed several calculations for screened potentials assuming different values of the physical parameters Z_1, v, and ω_P.

In Fig. 1 we show an example of the calculated values of the differential contributions to the transport cross section (DTCS) in Eq. (4) for the case $Z_1 = \pm 2$, $v = 2$ a.u., and $\omega_P = 0.5$ a.u. [atomic units (a.u.) are used in the following]. To illustrate the contributions from different impact parameters we show here the values of the DTCS, given classically by

$$F(b) \equiv d\sigma_{tr} = 2\pi b[1 - \cos(\theta_{(b)})], \tag{6}$$

according to Eq. (4), as a function of the impact parameter b.

The figure includes the results for $Z_1 = 2$ and $Z_1 = -2$ (solid lines) and the values corresponding to Rutherford scattering (dashed line), given by

$$F_{Ruth}(b) = 2\pi b[1 - \cos(\theta_R)] = \frac{4\pi b b_{cl}^2}{b^2 + b_{cl}^2}, \tag{7}$$

which is independent of the sign of Z_1. In addition, we show in the figure the values calculated using the small-angle approximation [20] (dotted line) given by

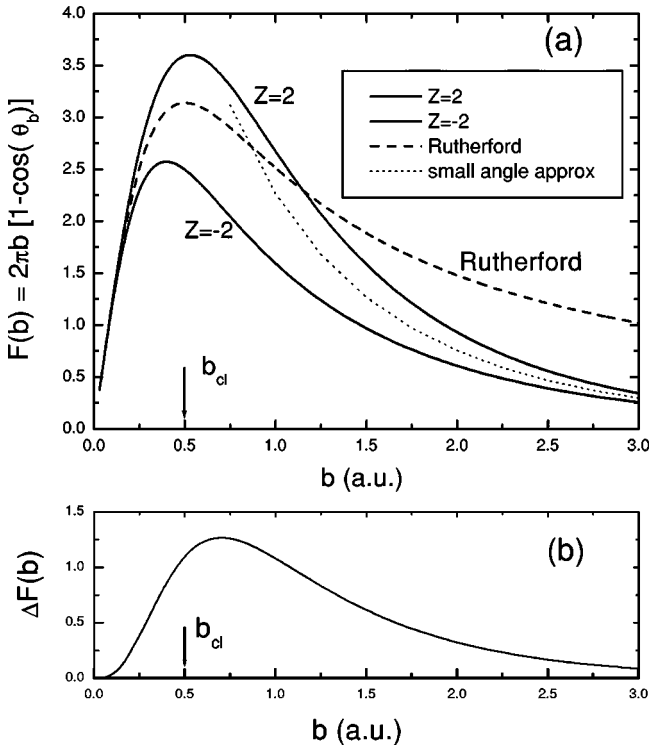

FIG. 1. Values of the differential transport cross section, Eq. (6), corresponding to electron scattering by positive and negative particles calculated by numerical integrations as described in the text (solid lines), together with the Rutherford values (dashed line) and the small-angle approximation (dotted line). (b) shows the difference between the two DTCS results, which represents the contribution from different impact parameters to the Barkas effect. The arrow indicates the classical collision radius $b_{cl}=|Z_1|e^2/mv^2$.

$$\theta_{small}(b) = -\frac{2}{v^2}\int_0^\infty \frac{\partial V(\sqrt{b^2+z^2})}{\partial b}dz, \tag{8}$$

which is independent of the sign of Z_1. The b_{cl} value indicated by an arrow in this figure is the classical radius, $b_{cl}=|Z_1|e^2/mv^2$.

In Fig. 1(b) we show the difference $\Delta F(b)=F(b)_+ - F(b)_-$ between the values for positive and negative charges. It shows that the maximum difference occurs for impact parameters close to b_{cl}, i.e., the typical range of close collisions.

The figure clearly shows that the accidental coincidence of the DTCS for positive and negative charges in the Rutherford picture (dashed line) is broken by the screening of the potential, yielding DTCS values larger for attractive than for repulsive fields. It should be noted that a qualitatively similar behavior has been found in Ref. [18] using a harmonic oscillator model. As we can clearly see in Fig. 1, these effects are localized in a range of distances close to b_{cl}, indicating the existence of Barkas effects in the range of close collisions.

It is of interest to note also some striking features arising from Fig. 1. First, one observes an enhancement of the DTCS for $Z>0$ (attractive field) for b values close to b_{cl}, which yields DTCS values for *screened* potentials *larger* than for a bare Coulomb potential (Rutherford scattering). This seemingly contradictory result may be physically explained by considering the changes in the *local* velocity of electrons as they approach the scattering center: for a Coulomb potential the electrons are accelerated as they fall into the attractive potential so that they arrive at close distances, $r\sim r_{min}$, with enhanced local velocities ($v_{local}>v$). Of course this effect is automatically included in the exact treatment of Rutherford scattering where the acceleration effect is maximum. But in the case of a screened potential this *prior acceleration* effect is smaller (due to the reduced interaction), and so the electrons arrive at points $r\sim r_{min}$ with relatively smaller velocities (as compared to "Rutherford electrons"). Therefore, they are more strongly scattered than Rutherford electrons.

For repulsive potentials ($Z_1<0$) the opposite effect takes place, and thus a reduction of the DTCS is obtained with respect to both the Rutherford and the attractive screened potential cases.

The previous explanation is actually not complete. There is also a geometrical effect related to the electron trajectories. For attractive interactions, the trajectories approaching the scattering center lead to distances of closest approach $r_{min}<b$, while the opposite occurs for repulsive interactions ($r_{min}>b$). For a Coulomb field, the differences in the scattering produced by these effects cancel out exactly with the previously mentioned effects of variations in the local velocities. Thus, for attractive interactions we get smaller values of r_{min} but larger values of v_{local}, whereas for repulsive fields we get larger values of r_{min} together with smaller values of v_{local}. As a result of a mutual cancellation of effects, the deflection angle corresponding to Rutherford scattering turns out to be independent of the sign of the field (i.e., of Z_1). But when the screening of the interaction is included the two (attractive and repulsive) cases split up, leading to different TCS results (Barkas effect).

We also note in Fig. 1 that the small-angle approximation Eq. (8) yields a good approximation to the exact results for $b\gg b_{cl}$. We observe that in this limit both results for $Z_1>0$ and $Z_1<0$ converge symmetrically to the small-angle approximation. This indicates the effect of Z_1^3 terms in the perturbative expansion, since the range $b\gg b_{cl}$ corresponds to the region where perturbation theory applies. It also indicates that the conditions for applicability of the Z_1^3 type of expansion to distant collisions may be more easily achieved than for close collisions.

III. TRANSPORT CROSS SECTION AND BARKAS EFFECT

From a large set of calculations of the type indicated before we have numerically integrated the TCS values for attractive and repulsive fields, and from these results we have determined the Barkas factor defined by Eq. (5).

In addition, we have performed numerical calculations of classical scattering trajectories in the asymmetric field of the dynamical potential obtained from the dielectric response formalism, calculated as indicated in Appendix A.

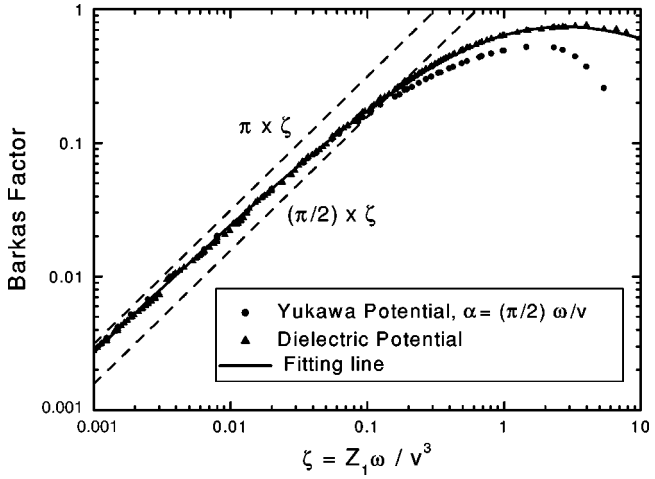

FIG. 2. Calculations of the Barkas factor defined by Eq. (5) for a Yukawa potential (circles) and for the dielectric potential (triangles) versus the parameter $\zeta=Z_1\omega_P/v^3$. The straight dashed lines show the approximations $R_{Barkas}\cong\pi\zeta$ and $R_{Barkas}\cong(\pi/2)\zeta$. As may be seen, the former approximation yields the correct limit for $\zeta\ll 1$. The solid line that goes through the triangles shows the results of Eq. (9) and fits all the values calculated using the dielectric potential.

The cylindrical potential $\phi_{scr}(\rho,z)$ from Eq. (A2) was first stored in a two-dimensional grid and the force components (parallel and perpendicular to the particle velocity) were calculated from the tabulated potential for each time step. Thus, the classical equations of motion were integrated to obtain the energy transfer to the target electron or the transport cross section.

The results of a large number of calculations are shown in Fig. 2, as a function of the parameter $\zeta=Z_1\omega_P/v^3$. The numerical values are indicated as data points, and include the two sets of calculations, using (a) the spherical average (circles) and (b) the whole dielectric potential (triangles). We find a very good convergence between the two sets of results over a wide range of ζ values, and a splitting of them in the high-ζ region. In addition, for $\zeta>1$ we find a saturation of the Barkas effect as well as a transition to a more complicated behavior.

The two straight lines shown in this figure are the values of the scaling parameter $gZ_1\omega_P/v^3$ in Eq. (3), using numerical factors $g=\pi$ and $g=\pi/2$. As may be observed, the convergence to the straight line behavior is extremely slow, so that one obtains the exact limit predicted by Lindhard, with $g=\pi$, only for very small values of ζ ($\zeta\sim 10^{-3}$). Instead, for $\zeta\sim 0.01$ the numerical results fall between the two lines, and for $\zeta\sim 0.1$ the results are closer to the line with $g=\pi/2$. This illustrates the difficulty in providing a unique quantitative prediction of the Barkas factor based only on scaling properties. It seems that this may in part explain earlier discrepancies in empirical evaluations of the role of close collisions in the Barkas effect.

In addition, we have included in this figure a fitting line given by the expression

$$G(\zeta)=\pi\zeta/(1+a\zeta^{0.25}+b\zeta+c\zeta^2) \tag{9}$$

with $a=0.92$, $b=2.75$, and $c=0.21$. This expression is shown by the solid line that goes through the set of triangle points, and yields an accurate fitting to all the numerical calculations obtained using the dielectric response function, on the whole range of values of interest here, $0.001<\zeta<10$, with an overall precision better than 5%. We think this analytical fit may be useful for practical estimations of the close collisions contribution to the Barkas effect.

We should also note that a correction factor $\pi/2$ was also introduced by Lindhard to account for deviations from the spherical symmetry of the induced potential. This would produce a total effect corresponding to $g=3\pi/2$. Our calculations for nonspherical potentials, however, do not support this additional correction. We also note that Lindhard's analysis did not indicate how large the departure from spherical symmetry should be in order to produce this further correction (this is of course a weak point in the argumentation). In fact, our results show a remarkably good agreement between both sets of calculations (using Yukawa and nonspherical dielectric potentials), showing that the spherical average is a very good approximation for this type of estimation in the range $\zeta<0.1$. It may be noted that here, as well as in Lindhard's estimation, second-order effects in the induced potential used for close collision calculations have been neglected.

In summary, our numerical results are in agreement with the value

$$R_{close}\cong 2B=\pi\zeta=\frac{\pi Z_1 e^2\omega_P}{mv^3}. \tag{10}$$

This result differs from $R_{dist}=(3\pi/2)Z_1e^2\omega_0/mv^3$ from the Ashley *et al.* theory [3], and implies that close and distant collisions contribute differently to the Barkas effect (i.e., there is no equipartition rule).

We finally note that the saturation observed for high values of B indicates the appearance of higher-order terms in the expansion of R_{Barkas} as a function of the charge Z_1. It also suggests the breakdown of the perturbative expansion for $B>1$. In this respect, we note that the present approach should be considered an all-order calculation since the scattering equations were numerically solved, with no perturbative assumptions at all.

IV. SUMMARY AND CONCLUSIONS

The contribution from close collisions to the Barkas effect proposed by Lindhard on the basis of general physical arguments was analyzed here in detail in the range of classical models. The original arguments as well as the scaling properties are essentially supported by these calculations.

The goal of this study was not to consider any particular application but to understand at a fundamental level the physics involved in the contribution of close collisions to the Barkas effect.

The effect of close collisions and the differences between attractive and repulsive fields have been shown by exact (nonperturbative) calculations of the differential transport cross sections.

The calculations serve to illustrate and clarify the origin of the Barkas differences in the range of close collisions. The main differences between particles and antiparticles arise in

fact from distances around the classical collision radius $b_{cl} = Z_1 e^2/mv^2$.

The most striking effect observed from the DTCS comparisons is the enhancement of the DTCS for an attractive screened potential as compared to the one for a pure Coulomb potential, which occurs at short collision distances, $r \sim b_{cl} = Z_1 e^2/mv^2$. This enhancement may be explained by considering the modification of the local velocities of scattered particles, i.e., by the same physical argument used by Lindhard to predict the Barkas effect in close collisions.

From the numerical evaluations of the DTCSs, we obtain the close-collision contribution to the Barkas effect, which satisfies the predicted scaling property with the parameter $Z_1 e^2 \omega_P / mv^3$.

The two sets of calculations, using either the asymmetric dynamical-screening potential or the spherical average of it, yield the same low-limit value of the Barkas factor in agreement with Lindhard's prediction (but without the additional nonspherical potential correction). In addition, we find a "saturation" of the Barkas effect for $B \sim 1$, which is related to higher-order terms in the scattering process, the present description being applicable to all orders of the interaction strength.

We finally note that the present considerations apply to the range of close collisions where the free electron picture may be regarded as a limiting approximation; this may include even nonmetallic targets in the high-energy range. For the treatment of the complementary range of distant collisions one may resort to the original ARB picture [3] which is characterized by the long-range polarization effect induced on the atomic shells.

ACKNOWLEDGMENTS

This work was supported in part by CONICET and ANPCYT of Argentina Grant No. (PICT03-03579), and the Bilateral Cooperation Program CAPES-SETCIP between Brazil and Argentina. Several useful comments by I. Nagy are gratefully acknowledged.

APPENDIX A: INDUCED POTENTIAL

We refer here to the calculation of the induced potential using the dielectric function formalism. Following Refs. [21,22] one obtains the expression for the induced potential for an ion moving along the z axis,

$$\phi_{ind}(\rho,z) = -Z_1 e \frac{v}{\pi} \int_0^\infty k dk J_0(k\rho) \int_{-\infty}^{+\infty} d\omega \frac{\exp(i\omega z/v)}{\omega^2 + k^2 v^2} \times \left[\frac{1}{\varepsilon(\omega)} - 1 \right]. \quad \text{(A1)}$$

Using the classical plasmon-pole approximation $\varepsilon(\omega) \cong 1 - \omega_P^2/\omega(\omega + i\gamma)$, with $\gamma \ll \omega_P$, and separating the real and imaginary parts of the dielectric function, we may separate ϕ_{ind} into a screening component ϕ_{scr} and a wake component ϕ_{wake} [21], where ϕ_{scr} is given by

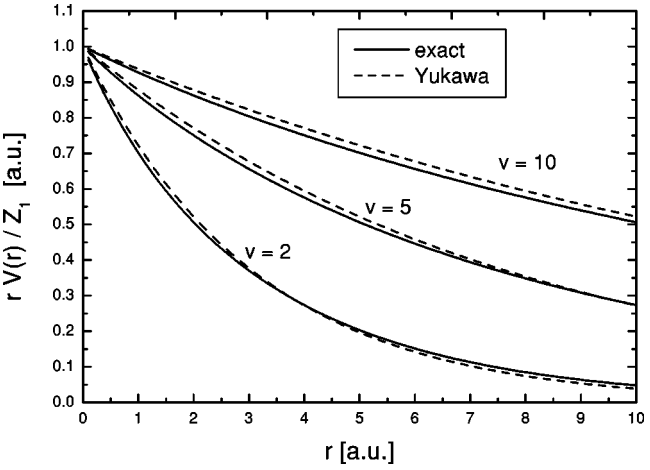

FIG. 3. Spherical average of the scattering potential, Eqs. (A3) and (A4), calculated using the dielectric function formalism for $v = 2$, 5, and 10 a.u., and Yukawa approximations $V(r) = -(Z_1 e^2/r) \exp(-\alpha r)$, with $\alpha = 1.3\omega_P/v$.

$$\phi_{scr}(\rho,z) = -Z_1 e \left(\frac{\omega_P}{v} \right)^2 \int_0^\infty \frac{J_0(k\rho)\exp(-k|z|)}{k^2 + \omega_P^2/v^2} dk \quad \text{(A2)}$$

and represents the dynamical screening of the moving ion by the dielectric medium. In Eq. (A2) ρ, z are the cylindrical coordinates relative to the instantaneous position of the ion (the induced potential is independent of the azimuthal angle φ).

On the other hand, the wake term ϕ_{wake} is related to collective (plasmon) excitations, which is a different mode of energy loss pertaining to the range of distant interactions not considered here [21,22]. (For the contribution of distant collisions to the Barkas effect we refer to the original article by Ashley *et al.* [3].)

From Eq. (A2) we can calculate the *spherical average* of the screening potential by performing the total angular average

$$\langle \phi_{scr} \rangle(r) = \langle \phi_{scr}(\rho,z,\varphi) \rangle = \frac{1}{4\pi} \int d\Omega \, \phi_{scr}(\rho,z,\varphi). \quad \text{(A3)}$$

Finally, to obtain the scattering potential we add the Coulomb potential of the bare ion,

$$\phi_{scat}(r) = \frac{Z_1 e}{r} + \langle \phi_{scr} \rangle(r). \quad \text{(A4)}$$

This yields the spherical average of the potential energy $V_s(r) = -e\phi_{scat}(r)$.

In Fig. 3 we compare the numerically averaged dielectric potential, Eq. (A4), with the Yukawa approximation $V(r) = -(Z_1 e^2/r) \exp(-\alpha r)$, where the screening constant scales with ion velocity as $\alpha = g\omega_P/v$. A very good approximation in the range of close distances is obtained with $g \cong 1.3$. The value suggested by Lindhard, $g = \pi/2$, has the advantage of yielding also the correct value for the energy shift, $\Delta V(0) = (\pi/2) Z_1 e^2 \omega_P / v$ in agreement with the dielectric theory. Hence, we used this value in the current evaluations.

The calculations reported in this paper have been made using two approaches: the first set of calculations were made using the spherical average approximation by a Yukawa potential, whereas the second set of calculations were made using the dielectric potential provided by Eq. (A2).

APPENDIX B: A SOLUBLE PROBLEM

A case that admits an exact analytical solution was noted by Nagy [23], who obtained the result for the so-called Mensing potential given by

$$V(r) = \begin{cases} -Z(1/r - 1/R), & r < R, \\ 0, & r > R, \end{cases} \tag{B1}$$

where R represents the screening distance. (Note that atomic units are used in this Appendix.)

The scattering angle θ for this potential is given, as a function of the impact parameter b, by [23,24]

$$\tan^2\left(\frac{\theta_b}{2}\right) = \left(\frac{Z}{bv^2}\right)^2 \frac{1-(b/R)^2}{[1-Z/(Rv^2)]^2}. \tag{B2}$$

Using this, one can readily obtain the differential transport cross section,

$$F(b) = 2\pi b[1-\cos(\theta_b)], \tag{B3}$$

and by integration one obtains the total transport cross section in the form

$$\sigma_{tr} = \frac{2\pi R^2}{(\lambda-1)^2}[\lambda\ln(\lambda) - (\lambda-1)] \tag{B4}$$

with

$$\lambda = \left(\frac{Rv^2}{Z} - 1\right)^2. \tag{B5}$$

The characteristics of the DTCS and TCS corresponding to this model are shown in Fig. 4. Panel (a) shows the impact parameter dependence of the DTCS, showing also the splitting of the cases with $Z>0$ and $Z<0$ with respect to the Rutherford value, as previously observed in Fig. 1.

Figure 4(b) shows the Barkas factor defined by Eq. (5), namely, $R_{Barkas}=\Delta\sigma_{tr}/2\langle\sigma_{tr}\rangle$. In this model R_{Barkas} scales with the parameter $\zeta=Z/Rv^2$. The dashed line here shows the line $R_{Barkas}=2Z/Rv^2$, which yields the limiting behavior for $Z/Rv^2\to 0$. Again, the results of this model are in good qualitative agreement with those of Fig. 2.

It is interesting to note that Lindhard [8] used an expression similar to Eq. (B2), namely,

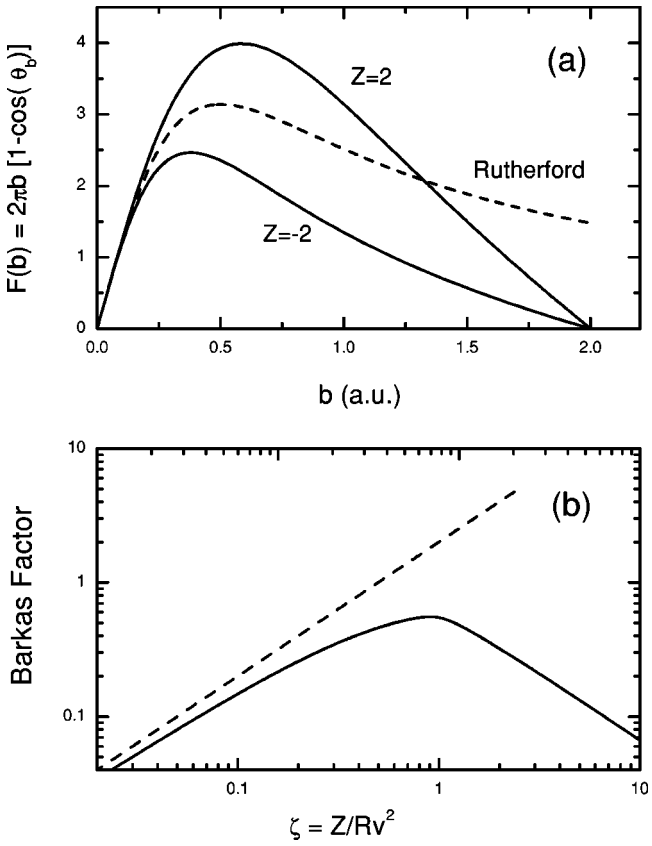

FIG. 4. (a) Differential transport cross section for the Mensing potential, for attractive and repulsive fields, given analytically by Eqs. (B2) and (B3), and Rutherford limit for unscreened fields. (b) shows the corresponding Barkas factor Eq. (5) for this case, which may be expressed analytically using Eqs. (B4) and (B5). The dashed line here yields the limit $R_{Barkas}^{Mensing}\cong 2\zeta=2Z/Rv^2$ corresponding to the present potential.

$$\tan^2\left(\frac{\theta_b}{2}\right) = \left(\frac{Z}{bv^2}\right)^2 \frac{1}{[1-Z/(Rv^2)]^2}, \tag{B6}$$

which is valid for $b\ll R$, to derive its Barkas-effect expression. Indeed, he assumed a constant offset of the incoming electron energy (in the projectile frame) of $\Delta V(0)=(\pi/2)Z_1e^2\omega_P/v$, which according to Eq. (B1) means $R^{-1}=(\pi/2)\omega_P/v$. Since the leading term of the Barkas factor, as can be calculated analytically from Eq. (B4), is $R_{Barkas}=2Z/Rv^2$, we easily get the Lindhard expression (without his extra *ad hoc* $\pi/2$ factor) $R_{Barkas}=\pi Z_1e^2\omega_P/mv^3$.

In summary, this simple model yields exact results, which serve to illustrate the general aspects of the behavior obtained from the calculations reported in Secs. II and III.

[1] W. H. Barkas, W. Birnbaum, and F. M. Smith, Phys. Rev. **101**, 778 (1956);W. H. Barkas, N. J. Dyer, and H. H. Heckman, Phys. Rev. Lett. **11**, 26 (1963).

[2] H. Bethe, Ann. Phys. (Leipzig) **5**, 325 (1930).

[3] J. C. Ashley, R. H. Ritchie, and W. Brandt, Bull. Am. Phys. Soc. **15**(1), 1338 (1970); Phys. Rev. B **5**, 2393 (1972).

[4] J. C. Ashley, R. H. Ritchie, and W. Brandt, Phys. Rev. A **8**, 2402 (1973); **10**, 737 (1974).

[5] J. D. Jackson and R. L. McCarthy, Phys. Rev. B **6**, 4132 (1972).
[6] K. W. Hill and E. Merzbacher, Phys. Rev. A **9**, 156 (1974).
[7] N. Bohr, Philos. Mag. **25**, 10 (1913).
[8] J. Lindhard, Nucl. Instrum. Methods **132**, 1 (1976).
[9] N. R. Arista, Phys. Rev. A **26**, 209 (1982).
[10] H. H. Mikkelsen and P. Sigmund, Phys. Rev. A **40**, 101 (1989); H. Esbensen and P. Sigmund, Ann. Phys. (N.Y.) **201**, 152 (1990).
[11] J. M. Pitarke, R. H. Ritchie, and P. M. Echenique, Phys. Rev. B **52**, 13 883 (1995).
[12] H. H. Andersen, H. Simonsen, and H. Sørensen, Nucl. Phys. A **125**, 171 (1969).
[13] H. H. Andersen, J. F. Bak, H. Knudsen, Nucl. Instrum. Methods **140**, 537 (1977).
[14] H. H. Andersen, J. F. Bak, H. Knudsen, and B. R. Nielsen, Phys. Rev. A **16**, 1929 (1977).
[15] H. Bichsel, Phys. Rev. A **41**, 3642 (1990).
[16] P. Sigmund, Nucl. Instrum. Methods Phys. Res. B **135**, 1 (1998).
[17] G. M. Azevedo, P. L. Grande, M. Behar, J. F. Días, and G. Schiwietz, Phys. Rev. Lett. **86**, 1482 (2001).
[18] M. M. Jakas, F. J. Pérez de la Rosa, and E. R. Custidiano, Phys. Rev. A **66**, 052902 (2002).
[19] A. F. Lifschitz and N. R. Arista, Phys. Rev. A **58**, 2168 (1998).
[20] J. Lindhard, V. Nielsen, and M. Scharff, K. Dan. Vidensk. Selsk. Mat. Fys. Medd. **36**, 1 (1968).
[21] P. M. Echenique, R. H. Ritchie, and W. Brandt, Phys. Rev. B **20**, 2567 (1979).
[22] I. Abril, R. García-Molina, C. D. Denton, F. J. Pérez, and N. R. Arista, Phys. Rev. A **58**, 357 (1998).
[23] I. Nagy, Nucl. Instrum. Methods Phys. Res. B **94**, 377 (1994).
[24] I. Nagy and B. Apagyi, in *Theory of the Interaction of Swift Ions with Matter*, edited by R. Cabrera-Trujillo and J. Sabin, Advances in Quantum Chemistry (Academic Press, New York, 2004).